

Magnetic Resonance Imaging Detection and Time Course of Cerebral Microhemorrhages during Passive Immunotherapy in Living Amyloid Precursor Protein Transgenic Mice

Feng Luo, Nathan R. Rustay, Terese Seifert, Beate Roesner, Vincent Hradil, Heinz Hillen, Ulrich Ebert, Jean M. Severin, Bryan F. Cox, Daniel A. Llano, Mark Day, and Gerard B. Fox

Translational Imaging and Biochemical Biomarkers (F.L., N.R.R., T.S., V.H., M.D., G.B.F.), Structural Biology (J.M.S), Integrative Pharmacology (B.F.C.), and Development Neuroscience (D.A.L.), Global Pharmaceutical Research and Development, Abbott Laboratories, Abbott Park, Illinois; and CNS Discovery Research, Abbott Laboratories, Ludwigshafen, Germany (B.R., H.H., U.E.)

Received July 14, 2010; accepted September 2, 2010

ABSTRACT

In recent years immunotherapy-based approaches for treating Alzheimer's disease have become the subject of intensive research. However, an important mechanistic-related safety concern is exacerbation of the risk of microhemorrhage that may be associated with fast removal of amyloid- β ($A\beta$) deposits found in blood vessels or brain parenchyma. Rapid in vivo detection of microhemorrhages in living amyloid precursor protein transgenic mice has not been described, and histological analysis can take several months before this risk is assessed. Aged transgenic mice were divided into two groups that would undergo longitudinal passive immunotherapy for 12 or 18 weeks. 6G1, a nonselective anti- $A\beta$ monoclonal antibody, and 8F5, a more selective antioligomeric $A\beta$ monoclonal antibody, were examined in both longitudinal studies. High-resolution T2*-weighted magnetic resonance microscopy ($100 \times 100 \times$

$400 \mu\text{m}$) was used for microhemorrhage detection in vivo. Cerebral microhemorrhages by magnetic resonance imaging were compared with histological hemosiderin staining in each animal; results showed that T2*-weighted magnetic resonance microscopy can reliably detect microhemorrhages of $\geq 60 \mu\text{m}$ in diameter at baseline and after 12 to 18 weeks of treatment in the same animals in vivo. This correlated significantly with histological readings. This new imaging safety biomarker can be readily applied to preclinical antibody screening in a longitudinal manner. 6G1 and 8F5, however, both increased microhemorrhage incidence in aged amyloid precursor protein transgenic mice compared with their baseline and vehicle treatment. A highly selective antibody for soluble $A\beta$ is needed to address the question of whether antibodies that do not bind to deposited $A\beta$ have microhemorrhage liability.

Introduction

Alzheimer's disease (AD) is the most common cause of dementia (Boche et al., 2008). According to the amyloid hypothesis, abnormal aggregation of amyloid- β ($A\beta$) in the brain triggers tau aggregation, microglial activation, synaptic dysfunction, and neuronal loss, ultimately resulting in cognitive decline (Hardy and Selkoe, 2002). $A\beta$ accumulates in the brains of patients with AD in the form of extracellular aggregates in the cerebral cortex and in the walls of blood vessels as cerebral amyloid angiopathy (CAA) (Boche et al.,

2008). Therefore, $A\beta$ represents an important molecular target for intervention in AD, and agents that can prevent its formation and accumulation or stimulate its clearance may ultimately be of therapeutic benefit (Schenk, 2002). Experimental studies of both active and passive $A\beta$ immunization in transgenic mice have confirmed that removal of existing $A\beta$ plaques can occur, sometimes within a matter of days, and this is associated with cognitive benefits (Schenk et al., 1999; Janus et al., 2000; Morgan et al., 2000; Schenk, 2002; Wilcock et al., 2004; Boche et al., 2008). However, several studies have demonstrated an increased incidence of cerebral microhemorrhages ex vivo in aged transgenic mice after a period of immunotherapy (Pfeifer et al., 2002; Racke et al., 2005; Wilcock et al., 2007; Schroeter et al., 2008; Thakker et al., 2009). The discontinued phase II active im-

This work was funded by Abbott Laboratories.
Article, publication date, and citation information can be found at
<http://jpet.aspetjournals.org>.
doi:10.1124/jpet.110.172932.

ABBREVIATIONS: AD, Alzheimer's disease; $A\beta$, β -amyloid; APP, amyloid precursor protein; CAA, cerebral amyloid angiopathy; FOV, field of view; MRI, magnetic resonance imaging; NBF, neutral buffered formalin; PBS, phosphate-buffered saline; TE, echo time; TR, repetition time.

munization trial with aggregated A β as an immunogen (AN1792) observed more severe CAA in immunized patients than those without at a similar stage of AD, with multiple cortical hemorrhages in one case (Boche et al., 2008; Thakker et al., 2009). Furthermore, microhemorrhage and dose-dependent vasogenic edema have been reported recently in patients with AD after passive immunization against A β (Salloway et al., 2009). These findings have significantly affected the clinical development of anti-amyloid immunotherapy platforms across industry and academia (Boche et al., 2008), and although the mechanism of vascular compromise is not known, both human and animal literature suggest that A β immunotherapy at least transiently worsens CAA (Thakker et al., 2009).

The analysis of microhemorrhage development may allow for improved safety profiles of potential immunotherapeutics. Although detection of small (20–400 μ M), individual microhemorrhages postmortem in mouse brain is possible by histological examination using Prussian blue (Pfeifer et al., 2002; Racke et al., 2005; Wilcock et al., 2007), it is very time consuming (Pfeifer et al., 2002; Wilcock et al., 2004; Racke et al., 2005; Schroeter et al., 2008). Two further fundamental questions cannot be easily addressed by using the *ex vivo* approach: 1) When do the microhemorrhages occur during immunotherapy? 2) Does age play a critical role in exacerbating cerebral microhemorrhages during immunotherapy? Thus, a new *in vivo* safety biomarker for monitoring microhemorrhage is needed. Given the promising data favoring efficacy of the anti-amyloid approach to the treatment of AD in animal models (Pfeifer et al., 2002; Racke et al., 2005; Wilcock et al., 2007; Schroeter et al., 2008; Thakker et al., 2009) it will be of great value to develop a rapid and highly sensitive method for preclinically screening potential immunotherapeutic compounds for their potential to cause vascular compromise.

MRI microscopy is capable of assessing the global anatomical status of rodent brains because it can provide a three-dimensional data set of the entire brain without sectioning. However, MRI-based techniques have the significant limitation of decreased image resolution compared with *ex vivo* histology. To apply MRI microscopy to the detection of cerebral microhemorrhage in living transgenic mice, one must determine whether it can provide sufficient resolution and contrast to identify the microhemorrhage. In this article, we report the first identification of cerebral microhemorrhage in living APP Swedish transgenic mice by using T2*-weighted MRI microscopy with an in-plane resolution of 100 μ m. A Prussian blue histological readout was also acquired after the imaging endpoint. The fast removal of deposited A β from the brain vasculature has been hypothesized to be a cause of microhemorrhage. Therefore, strategies that target soluble oligomers and avoid the removal of insoluble A β plaques, which are heavily involved in CAA, have been proposed (Barghorn et al., 2005) to be a potentially safer and more effective treatment for AD than nonspecific removal of multiple species of A β . To test the hypothesis that fewer microhemorrhages will occur when soluble A β oligomers are targeted (reducing the removal of insoluble A β plaques in the vessel walls), two different anti-A β monoclonal antibodies were used in two longitudinal studies in aged Tg2576 mice. A nonselective antibody targeting soluble and insoluble A β

(6G1) and a more selective antioligomer antibody (8F5) were used (Barghorn et al., 2005).

Materials and Methods

Initial Control Study

Seven male C57BL/6 mice (approximately 3–6 months old at the time of imaging), purchased from Taconic Farms (Germantown, NY), were used in control studies to determine the feasibility of using MRI to detect hemosiderin deposits *in vivo*. Hemosiderin deposits result from the phagocytosis of hemoglobin by macrophages and are used as a histological marker of hemorrhage. In these studies, mice were anesthetized with 2.5% isoflurane in oxygen and placed into a small animal stereotaxic adapter (Stoelting, Chicago, IL) fitted to a larger stereotaxic frame (David Kopf Instruments, Tujunga, CA). A midline scalp incision was made by using sterile surgical techniques, and 0.1 μ l of whole arterial blood was microinjected intracerebrally via a burr hole to deliver to a point at the cortical and subcortical junction (coordinates from bregma: anterior posterior, -1.7 mm; mediolateral, 1.0 mm; dorsal-ventral, 2.5 mm; dorsal-ventral set at 2.5 mm to allow for needle bevel). Donor arterial blood was obtained fresh from seven additional male mice (Taconic Farms) from the carotid artery under terminal isoflurane anesthesia.

Transgenic Mice

A total of 60 heterozygous double Swedish mutation (K670N and M671L) Tg2576 transgenic mice that express human APP cDNA (Hsiao et al., 1996; Spire and Hyman, 2005) were obtained from Taconic Farms at approximately 3 months of age. Mice were imaged at approximately 17 to 23 months of age. In the 12-week passive immunotherapy study, 30 male and female Tg2576 mice underwent baseline MRI scan at the age of 19 months, followed by 12 weekly intraperitoneal injections of vehicle [phosphate-buffered saline (PBS)], antibody 6G1 (0.5 mg/mouse/week in 0.1 ml of PBS), or antibody 8F5 (0.5 mg/mouse/week in 0.1 ml of PBS), with 10 mice per group (Fig. 1). In the 18-week passive immunotherapy study, another 30 male Tg2576 mice underwent a baseline MRI scan at the age of 17 months followed by 18 weeks of weekly treatment with antibody 8F5 (0.5 mg/mouse/week in 0.1 ml of PBS) or control antibody IgG_{2a} (0.5 mg/mouse/week in 0.1 ml of PBS) (Fig. 1). Passive vaccination was commenced within 1 week of completion of baseline MRI acquisition. Female mice were group-housed and male mice were single-housed in filtered isolation cages initially and then transferred to a filtered, forced-air isolation rack. All mice were maintained on standard sterile wood chip bedding in a quiet room under conditions of 12-h lights on/12-h lights off (on at 6:00 AM), with food and water available *ad libitum*. An electronic chip, IMI-1000 from Bio Medical Data Systems (Seaford, DE), was implanted subcutaneously in the dorsal posterior region for identification purposes. This chip was removed before final MRI scanning. All imaging was performed during the light phase, and all experiments were conducted in accordance with the Abbott Institutional Animal Care and Use Committee and the National Institutes of Health *Guide for Care and Use of Laboratory Animals* in facilities accredited by the Association for the Assessment and Accreditation of Laboratory Animal Care.

MRI Methodology

MRI experiments were carried out by using a Bruker BioSpin horizontal-bore scanner (7.0 T/21 cm, 300 MHz) (Bruker BioSpin, Ettlingen, Germany) equipped with a triple-axis gradient unit (maximum 40 G/cm per direction). Animals were first anesthetized with medetomidine hydrochloride (Domitor, 1 mg/kg *i.p.*; Pfizer Animal Health, Exton, PA) + ketamine (75 mg/kg *i.p.*; Fort Dodge Animal Health, Fort Dodge, IA) (Luo et al., 2008) and then placed in a dual-coil small animal restrainer (Insight Neuroimaging Systems, LLC, Worcester, MA), which contains a volume coil for transmitting

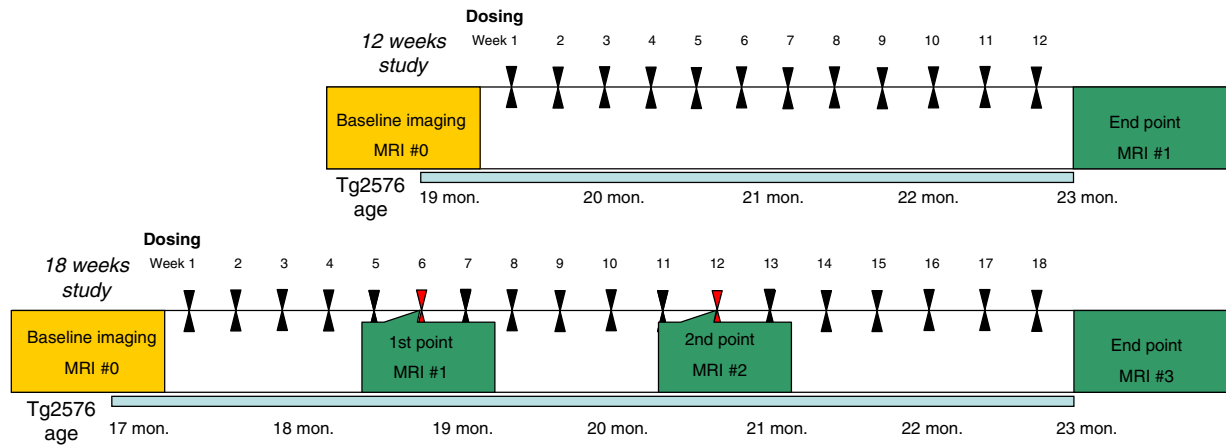


Fig. 1. Imaging study paradigms. The two longitudinal study paradigms are illustrated. Multiple MRI readouts were used in the 18-week imaging study (bottom), whereas 1 MRI readout was used in the 12-week study (top). Although the same age (~23 months old) Tg2576 was used for the endpoint image acquisition in both longitudinal studies, animals used in the 18-week study were approximately 2 months younger at the beginning of assessment.

and a surface coil for receiving. Respiration rates and waveforms were continuously monitored via a force transducer. Rectal temperature was monitored and maintained at $37 \pm 1^\circ\text{C}$ via a feedback-regulated, circulating water pad. For longitudinal imaging studies, medetomidine anesthesia was reversed by intraperitoneal injection of atipamezole (0.1 mg/kg; Antisedan; Pfizer, Karlsruhe, Germany) at the end of each imaging session (Weber et al., 2006). Coil-to-coil electromagnetic interaction was actively decoupled. Multislice, multi-echo pulse sequence with TR/TE = 500/11 ms, bandwidth = 2700 Hz, FOV = 2.56×2.56 cm, imaging matrix = 256×256 , and six averages was used for T1 anatomical images for eight 1-mm slices. Rapid acquisition relaxation enhanced pulse sequence with TR/TE = 3000/50 ms, bandwidth = 5400 Hz, FOV = 2.56×2.56 cm, matrix = 256×256 , rapid acquisition relaxation enhanced factor = 8, and four averages was used for T2 anatomical images for eight 1.0-mm slices. In-plane resolution for T1 and T2 anatomical images were 100×100 μm and covered the range of interaural 6.0 to -1.0 mm. A gradient echo three-dimensional fast low-angle shot sequence with TR/TE = 100/13 ms, bandwidth = 22,000 Hz, FOV = 2.56×2.56 cm, imaging matrix = $256 \times 256 \times 16$, and four averages was used for T2* anatomical images with in-plane resolution = 100×100 μm and interplane resolution = 400 μm and covered the range of approximately interaural 6.0 to 0.0 mm. After intracerebral microinjection of whole arterial blood in the initial control studies, acute scans were obtained from all seven mice within 30 min. Of these, three mice were perfusion-fixed for subsequent histological assessment and identification of acute "hemorrhage." The remaining four mice were housed for an additional 14 days, at which point two of the mice were rescanned for identification of hemosiderin deposits resulting from the initial injection. After MRI, these mice and the remaining two mice were perfusion-fixed for histochemical confirmation of hemosiderin deposits. Ex vivo T2*-weighted MRI microscopy was conducted after in vivo imaging in the same animal for the 12-week longitudinal study. Thorough cardiac perfusion was used to eradicate blood flow void signal in the ex vivo setting. For the 18-week longitudinal MRI study, multiple time-point MRI readouts were collected at 6, 12, and 18 weeks after baseline acquisition. The paradigms for the 12- and 18-week longitudinal MRI studies are illustrated in Fig. 1.

Histology

Initial Control Studies. For the initial control studies, three mice that were microinjected with arterial blood were euthanized with 100% CO_2 , 2 h after the microinjection (after the initial MRI scan). Brains were removed and immersion-fixed in neutral buffered formalin (NBF). After paraffin embedding, sectioning was conducted

on a microtome at 6- μm slice thickness. Hematoxylin and eosin staining was used to visualize the acute hemorrhage. Detection of acute hemorrhage via histology was compared with MRI images in the same area. Perl's Prussian blue staining was used to identify hemosiderin deposits in the remaining four normal C57BL/6 mice 14 days after blood microinjection. Detection of chronic hemorrhage using MRI was compared with histology in each animal.

Twelve- and 18-Week Longitudinal Studies. For the two longitudinal studies, after the last in-life MRI scan, each mouse was deeply anesthetized with medetomidine/xylazine and perfused with ice-cold PBS at a rate of 5.0 ml/min for 2.5 min via the left atrium by using an open thorax method. The right atrium was cut at the start of the perfusion. Each mouse was then perfusion-fixed with 10% NBF at a rate of 5 ml/min for 5.5 min. For the first 12-week immunotherapy study, the brain was removed from each mouse, cut into two hemispheres, and postfixed in 10% NBF overnight. Brains were subsequently cryoprotected by placement in a solution of 30% sucrose for approximately 2 days (until the brain hemispheres had fallen to the bottom of the vial) and stored at 4°C until sectioning. Brains were sectioned at 30 μm with a cryostat. The right hemisphere was sectioned in the coronal plane, and the left hemisphere was sectioned in the horizontal plane. A total of eight series of sections were cut. One series of sections was stained with Perl's Prussian blue to identify hemosiderin deposits resulting from microhemorrhages and counterstained with neutral red. An arbitrary 60 μm was used to categorize Prussian blue-positive lesions into two pools: number of all lesions versus number of lesion with size ≥ 60 μm . This was based on control studies that indicated this may be a possible detection size limit for our MRI protocol. An adjacent series of sections was stained with Congo red to identify A β deposits. The remaining six series of sections were stored for alternative future histochemical analyses. Thus, there was approximately 240 μm (30 $\mu\text{m} \times$ eight series) between each section analyzed. For the second 18-week passive immunization study, the whole brain was sectioned in the coronal plane; otherwise the same histological preparation was used.

Antibodies

Antibodies were produced at Abbott Laboratories (Structural Biology, Advanced Technology, Abbott Park, IL). Monoclonal antibodies 6G1 and 8F5 were generated from mice immunized with A β_{1-42} globulomer according to standard procedures (Barghorn et al., 2005). Antibody 8F5 is reported to be approximately 100 times more selective than 6G1 for soluble A β oligomers (Barghorn et al., 2005). In brief, anti-A β mAb ML5-6G1.3E2.5C3 (molecular mass 150 kDa) was produced by fermentation in 25-liter wave bags, purified of most

endotoxin (approximately 1 EU/mg remained), and provided in a volume of 57 ml and a concentration of 0.96 mg/ml in PBS at pH 7.4. Anti-A β mAb ML5–8F5 (molecular mass 148 kDa) was produced by fermentation in 10-liter wave bags, purified of endotoxin, and provided in a volume of 20 ml and a concentration of 1.65 mg/ml in PBS at pH 7.4. IgG_{2a}, 35 ml at a concentration of 7.03 mg/ml, was produced by Abbott Laboratories (Structural Biology, Advanced Technology) and used as a negative control for 8F5 in the second 18-week vaccination study. Antibody solutions were diluted under sterile conditions in PBS pH 7.4 and aliquoted into sterile tubes and stored at 4°C until use. All solutions were prepared fresh on the day of injection. Each transgenic mouse was dosed with 0.5 mg/week i.p.

Data Analysis

Microhemorrhage incidence identified by MRI was determined by two independent, blinded investigators after the completion of the in-life portion of the study. This was conducted by reviewing scans on the console monitor in the imaging laboratory in a blinded manner over 4 to 6 h. Scorers were first trained to examine “normal,” non-pathological MRI data from young, healthy mice. This was done to get accustomed to the typical hyperintensities and hypointensities that are present in T2*-weighted scans. Because microhemorrhage signals often present asymmetrically in the brain, bilateral signals in congruent brain regions were usually excluded from microhemorrhage quantification. Microhemorrhage incidence identified by histology was also determined by two investigators using the postmortem tissue sections. This was conducted in a blinded manner over a full 30-day period using a light microscope (Nikon, Tokyo, Japan). Each section on each slide was evaluated separately in a grid pattern (left to right, top to bottom) under 60 \times (6 \times objective lens, 10 \times eyepiece lens) magnification. Higher magnification (120 \times , 240 \times) was used for clarification of unclear points of interest. Microhemorrhages were counted on a per-site basis in Prussian blue-stained sections. Using a stage micrometer, the estimated size, location, and nature (intensity of staining) of each cluster site was individually recorded. To account for differences in every cluster site that could contain several hemosiderin deposits close together or spread further apart, microhemorrhage data collected by histology were transformed into microhemorrhage scores (Pfeifer et al., 2002; Racke et al., 2005), based on the number of hemosiderin-positive cells detected in each deposit. Each deposit was rated with a score of 1 to 3 based on the following criteria: 1 = one to three hemosiderin-positive cells, 2 = four to 10 hemosiderin-positive cells, and 3 = >10 hemosiderin-positive cells. Each mouse’s microhemorrhage score was calculated by multiplying the rating of each deposit by the total number of deposits, which provided a general estimate of the extent of microhemorrhage (Pfeifer et al., 2002; Racke et al., 2005). All calculations were made by using Prism version 4.0 for Windows (GraphPad Software Inc., San Diego, CA). Quantified microhemorrhage data were analyzed by one- or two-way analysis of variance (with repeated-measures where appropriate), and significant main effects and interactions were analyzed by Bonferroni post hoc tests. An α level of $p < 0.05$ was set for statistical significance.

Results

Initial Control Study. Detection of acute (Fig. 2) and chronic (Fig. 3) microhemorrhages in naive mouse brain was demonstrated after microinjecting small volumes (0.1 μ l) of arterial blood intracerebrally by using MRI and histology. Artificial “cerebral microhemorrhage” was clearly visible immediately (Fig. 2) and 14 days (Fig. 3) after the initial microinjection of whole blood by T2*-weighted MRI microscopy, but not by T1- or T2-weighted MRI. The blood-generated hypointense MRI signal was colocalized with red blood cells at the acute phase (immediate) and with hemosiderin deposit

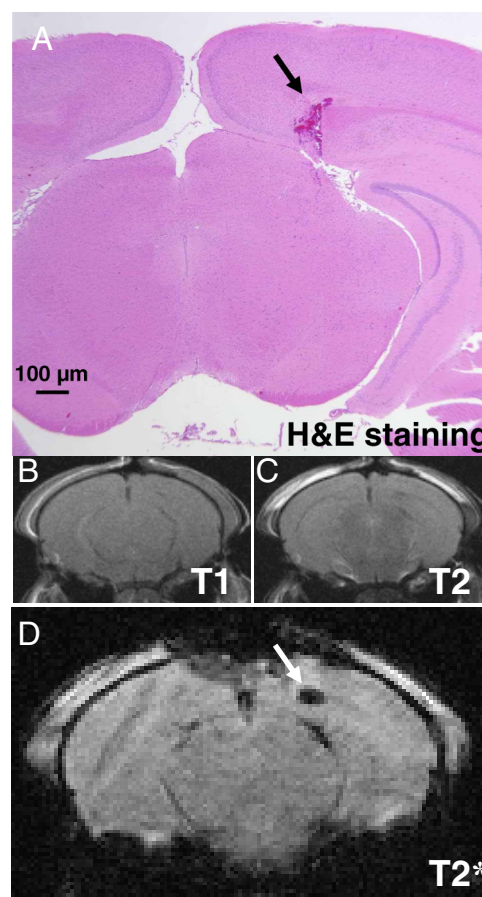


Fig. 2. Control study: acute detection of artificial microhemorrhage in naive mice using MRI and histology. A, hematoxylin and eosin staining. B, T1-weighted MRI. C, T2-weighted MRI. D, T2*-weighted MRI. Arrows indicate site of microinjection of whole blood (volume 0.1 μ l). MRI scans were taken within 30 min of microinjection of whole blood.

at the chronic phase (14 days after injection). These dark signals persist after eliminating any blood flow void effect by imaging again after cardiac perfusion (Fig. 3I).

Twelve-Week Longitudinal Study. A maximum of one to two probable cerebral microhemorrhage signals were observed at baseline in 19-month-old transgenic animals before any treatment (Fig. 4). One mouse with four microhemorrhages at baseline was excluded from analysis, but was treated with 8F5 and followed to the final imaging assessment. Monoclonal antibodies 6G1 and 8F5 increased the incidence of microhemorrhages after 12 weeks of treatment (Figs. 4 and 5, respectively) in both coronal and horizontal MRI planes. Subsequent Prussian blue histochemistry revealed hemosiderin deposits (Fig. 5, B–D) at many of the sites identified in MRI scans in vivo (Fig. 5A). Quantification of MRI-identified microhemorrhages corroborates histochemistry findings and revealed a significant increase after 12 weeks of treatment with 6G1 and 8F5 compared with their own baseline (Fig. 6A). This was supported by a significant main effect of time ($F_{1,18} = 21.68$; $p < 0.001$), demonstrating higher numbers of microhemorrhages at the 12-week time point, and a significant treatment \times time interaction ($F_{2,18} = 4.39$; $p < 0.05$). Bonferroni post hoc testing of this interaction revealed that both 6G1 ($p < 0.05$) and 8F5 ($p < 0.01$) treatment significantly increased the number of microhemorrhages compared with vehicle treatment. No increase in

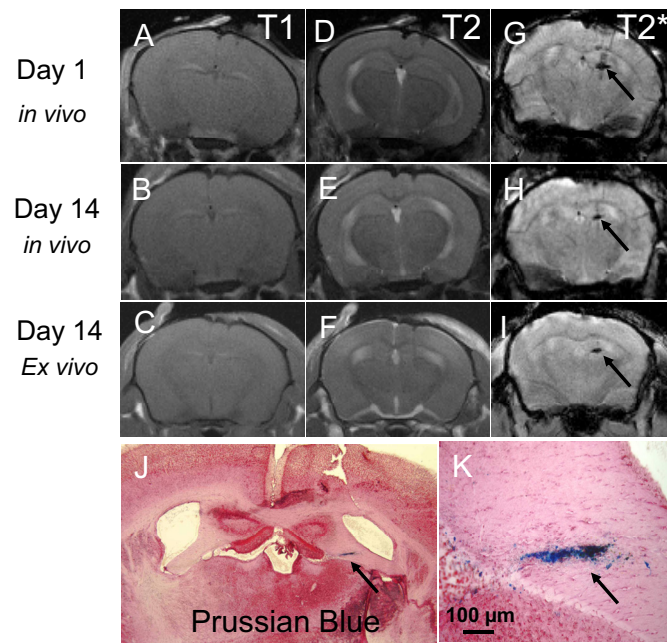


Fig. 3. Control study: detection of artificial microhemorrhage in naive mice using MRI and histology 14 days after microinjection. A–C, T1-weighted MRI. D–F, T2-weighted MRI. G–I, T2*-weighted MRI at days indicated after microinjection of whole blood. Images in A, D, and G were acquired 1 day after microinjection of blood, and images in B, E, and H were acquired 14 days after microinjection of blood in live animals. After thorough cardiac perfusion, the same animals were scanned by MRI again (C, F, and I). J and K, Prussian blue histochemical staining of hem siderin deposits resulting from artificial microhemorrhage at 14 days after microinjection of whole blood. Arrows indicate site of microinjection of whole blood (volume 0.1 μ l) at 15 \times (J) and 120 \times (K).

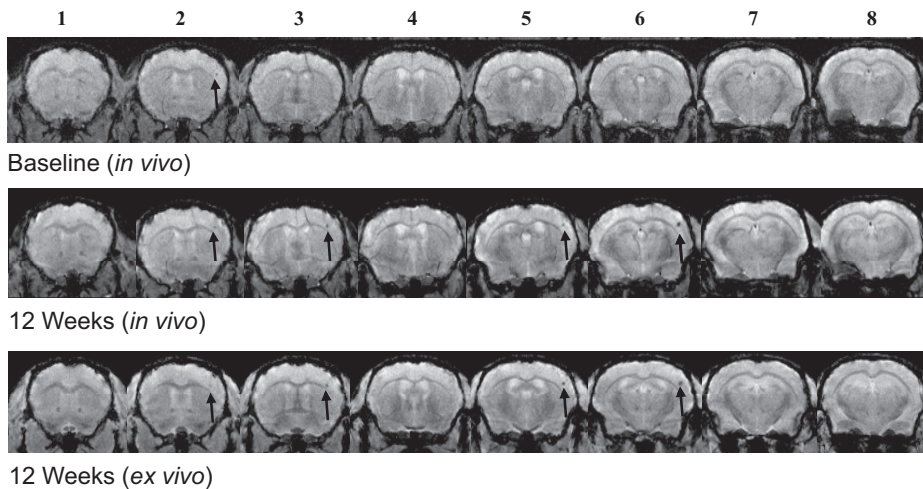


Fig. 4. Example of microhemorrhages in cortex across multiple MRI slices (1–8) after 12-week treatment with mAb 6G1 (1–8). T2*-weighted coronal MRI scans at baseline or after 12 weeks of 6G1 treatment. Only eight coronal slices are shown in this example from a total of 16 taken. In vivo indicates MRI scans taken just before the end of the study. Ex vivo indicates MRI scans taken after cardiac perfusion fixation. Arrows indicate microhemorrhages visible to T2*-weighted MRI.

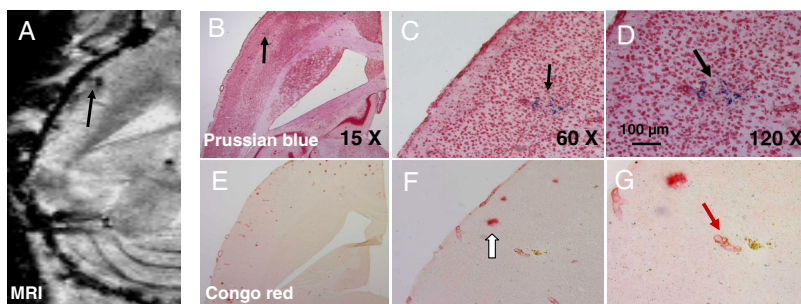


Fig. 5. Example of microhemorrhage in cortex after 12-week treatment of mAb 8F5. A, in vivo T2*-weighted MRI in the horizontal plane. B–D, Prussian blue/neutral red histochemical staining of a cluster of hem siderin deposits postmortem in the same brain at different magnifications. Hem siderin-positive cells are illustrated under higher magnification (black arrows). E–G, Congo red staining on an adjacent series of brain tissue sections (30 μ m apart) shows Congo red-positive staining vessel proximal to hem siderin-positive cells (red arrow). Multiple A β deposits are visible in cortex (hollow arrow) by Congo red staining.

hemorrhage incidence was seen after 12 weeks of treatment with PBS (Fig. 6A). This increase by 6G1 and 8F5 was also the case when microhemorrhages $>60 \mu$ m were quantified (Fig. 6B). Quantification of histochemistry-identified microhemorrhages also showed increased microhemorrhages in the 8F5 and 6G1 treatment groups compared with mice treated with vehicle (Fig. 6C). Mice treated with 8F5 showed significantly more microhemorrhages compared with vehicle ($p < 0.05$), whereas mice treated with 6G1 showed a similar trend ($p = 0.08$). It is important to note that the one mouse, which was excluded at the beginning of the study because of more than four microhemorrhages at baseline, revealed more than 20 microhemorrhages after 12 weeks of 8F5 treatment (Fig. 9).

Eighteen-Week Longitudinal Study. A maximum of one to two probable cerebral microhemorrhage signals were observed at baseline in 17-month-old transgenic animals before any treatment. Figure 7 illustrates the quantification of microhemorrhages from the individual MRI time points during the 18 weeks of 8F5 and IgG_{2a} treatment. For the MRI data, a main effect of time was detected ($F_{3,18} = 6.65$; $p < 0.001$), suggesting an overall increase in microhemorrhages as treatment progressed. For the initial 6 and 12 weeks of treatment, no significant increase of microhemorrhages was found in the 8F5 treatment group; however, Bonferroni post hoc testing revealed a significant increase of cerebral microhemorrhages at 18 weeks in the 8F5 treatment group compared with IgG_{2a} ($p < 0.05$; Fig. 7). Quantification of histochemistry-identified microhemorrhages with lesion size $\geq 60 \mu$ m corroborates our MRI findings in that significantly more microhemorrhages were detected in 8F5 treatment groups compared the mice treated with IgG_{2a} ($p < 0.05$; Fig. 7).

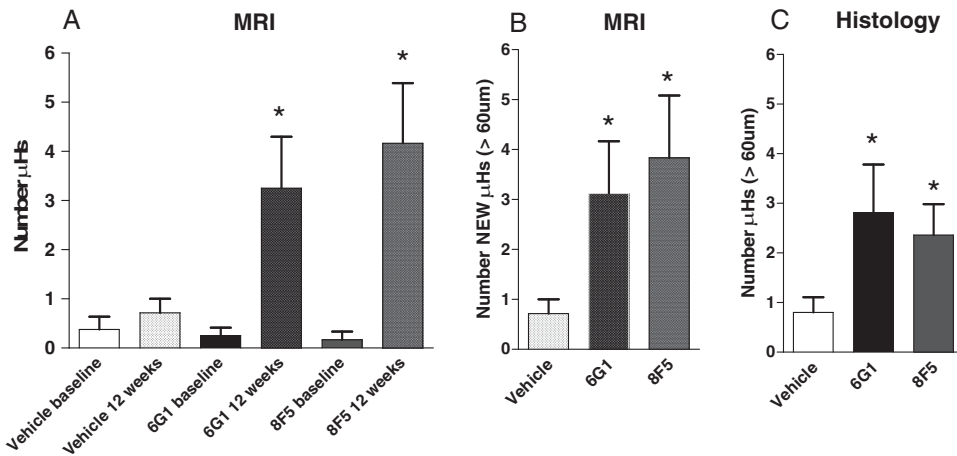


Fig. 6. A, MRI findings of microhemorrhages are illustrated (mean \pm S.E.M.) at baseline and after 12 weeks of treatment with vehicle, 6G1, and 8F5. B, number of new μ H $>60 \mu$ m detected by MRI after 12 weeks of treatment. C, histology: quantification of microhemorrhage (mean \pm S.E.M.) with lesion size $\geq 60 \mu$ m after 12-week treatment of vehicle, 6G1, and 8F5 is illustrated. *, $P < 0.05$ compared with vehicle at 12-week time point (Bonferroni post hoc test).

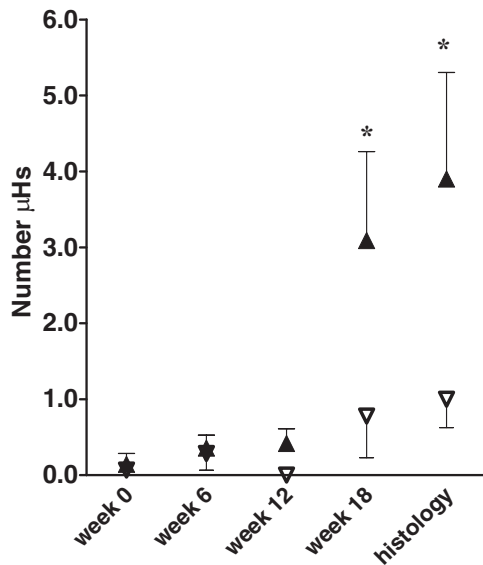


Fig. 7. Time course of MRI findings of microhemorrhage (mean \pm S.E.M.) at baseline, 6 weeks, 12 weeks, and 18 weeks in IgG_{2a} or 8F5 treatment groups. ▲, 8F5, ▽, IgG_{2a}. Histology: quantification of microhemorrhage (mean \pm S.E.M.) with lesion size $\geq 60 \mu$ m after 18-week treatment of IgG_{2a} or 8F5 is shown. *, $P < 0.05$ compared with IgG_{2a} (Bonferroni post hoc test) for MRI data or IgG_{2a} (one-tailed t test) for histology data.

Correlation of MRI and Histology. Figure 8 shows the correlation plot for microhemorrhage findings by MRI and histology in the two longitudinal studies. A significant correlation was observed for all microhemorrhages identified by histology versus microhemorrhages identified by MRI ($r^2 = 0.5492$; $p < 0.0001$). An improved correlation was found when plotting lesion size $\geq 60 \mu$ m identified by histology versus MRI findings ($r^2 = 0.7511$; $p < 0.0001$). Noticeably, a near 1:1 ratio was observed in Fig. 8B, which implies that microhemorrhages of $\geq 60 \mu$ m are quite likely to be detected by T2*-weighted MR microscopy using our current protocol.

Discussion

An independent safety monitoring committee has found that patients with AD given the highest dose of an experimental monoclonal antibody, bapineuzumab, were more likely to develop cerebral vasogenic edema; the highest dose was subsequently discontinued from the clinical trial (Salloway et al., 2009). The Food and Drug Administration has also

posted concerns regarding the safety of immunotherapy approaches, stating that microhemorrhage susceptibility is a risk factor for vasogenic edema. This highlights the importance of such safety assessments while developing immunotherapy strategies for the treatment of AD.

Although the diagnosis of microhemorrhages in human brain by gradient-echo sequence or T2*-weighted MRI (Offenbacher et al., 1996; Fazekas et al., 1999; Greenberg et al., 2004) has been established, the preclinical identification of cerebral microhemorrhage is challenging because microhemorrhage in a mouse brain is approximately two orders of magnitude smaller (in the range 20 to 400 μ m) than that found in human brain (<5 mm in size) (Viswanathan and Chabriat, 2006). In our initial control study, we demonstrated the feasibility of detecting cerebral microhemorrhage in living transgenic mice. We were able to visualize a hypointense MRI signal immediately after microinjection of 0.1 μ l of arterial blood, which represents the proposed upper limit of microhemorrhage size (400 \times 400 \times 500 μ m³) induced by immunotherapy in aged transgenic mice (Pfeifer et al., 2002; Racke et al., 2005; Wilcock et al., 2007; Thakker et al., 2009). Second, we observed the hypointense MRI signal 14 days after exogenous blood injection, which remained even after perfusion of the brain with PBS. Although deoxygenated blood signal may contribute to the hypointensity MRI finding in the acute phase (Linfante et al., 1999), hemosiderin deposits after macrophage phagocytosis of red blood cells (Bradley, 1993; Viswanathan and Chabriat, 2006) during the chronic phase of bleeding results in the hypointense signal in T2*-weighted MRI demonstrated in Fig. 2. That the hypointense MRI signal is detectable at the location of blood microinjection even after 14 days rules out the possibility of a vascular flow void effect (Fig. 2) and is supported by the detection of hemosiderin deposits via Prussian blue histochemistry (Bradley, 1993; Viswanathan and Chabriat, 2006).

Immunotherapy-induced cerebral microhemorrhages were detected in aged living transgenic mice by T2*-weighted MRI microscopy (Figs. 4–6). Support for the use of MRI for detection of microhemorrhages comes from the fact that those identified by MRI microscopy quite often colocalized with those determined by histology. It is important to note that a point-to-point comparison between histology and MRI is not feasible (Jack et al., 2004), because of the different in-plane and interplane resolution used in MRI (in-plane: 100 \times 100 μ m; interplane: 400 μ m) and histology (in-plane: ∞ ; inter-

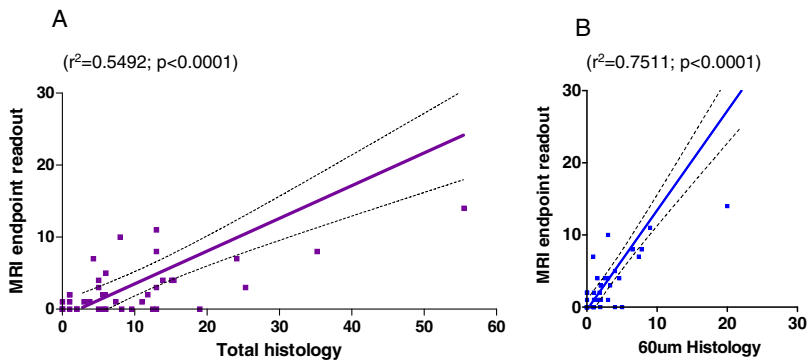


Fig. 8. Correlation of MRI and histology in two longitudinal studies. A, MRI quantification of microhemorrhages versus histology quantification of all detectable microhemorrhages. B, MRI quantification of microhemorrhages versus histology quantification of microhemorrhages with lesion size $\geq 60 \mu\text{m}$.

plane: $240 \mu\text{m}$). Because of this, there is not a perfect slice-to-slice comparison for MRI and histology. Nevertheless, our findings in histology significantly correlated with MRI findings in the current data set (Fig. 8), and one might speculate an improved correlation if entire histology sections were used.

There is the potential that hypointensities found in T2 or T2*-weighted MRI microscopy could be attributed to A β plaques in transgenic mice (Jack et al., 2004; Lee et al., 2004; Zhang et al., 2004). This is unlikely in our study, because we did not use an extremely high resolution in MRI ($100 \mu\text{m}$ versus ~ 50 to $60 \mu\text{m}$; Jack et al., 2004; Lee et al., 2004; Zhang et al., 2004) as is required for potential interference by A β plaques. Sigurdsson et al. (2008) have shown that very large plaque deposits are detectable in aged Tg2576 mice via T2*-weighted MRI at $100\text{-}\mu\text{m}$ resolution. However, given the size of the plaques detected by Congo red in our work (Fig. 5), which seem smaller than $100 \mu\text{m}$ (the reported maximal plaque size in mice; Jack et al., 2004), we do not believe that many plaques would be detected by MRI in our studies. In addition, there was a greater correspondence between the location of MR hypointensities and hemosiderin deposits; Congo red-positive plaques tended not to colocalize with hemosiderin deposits (see Fig. 5).

Although we were able to successfully implement the use of T2*-weighted MRI microscopy to identify cerebral microhemorrhage in living mouse brain, the mechanisms of anti-A β immunotherapy-induced microhemorrhages in aged transgenic mice are still not fully understood. Although we replicated the effect of monoclonal mouse antibody 6G1 (structurally equivalent to antibody 6E10; see Barghorn et al., 2005)

to exacerbate cerebral microhemorrhages in aged transgenic mice (Thakker et al., 2009), 8F5, a more selective antibody to soluble oligomers, was also associated with cerebral microhemorrhage examined in the first and confirmed in the second longitudinal study (Figs. 6 and 7). It is possible that because of the high relative concentration of insoluble to soluble A β in the brain of Tg2576 mice at older ages (Kawarabayashi et al., 2001) that the more selective antibody 8F5 demonstrated some nonspecific binding to fibrillar A β and the vasculature. This may have contributed to the similar effects on microhemorrhage production in both 6G1- and 8F5-treated groups.

A study by Racke et al. (2005) demonstrated that the occurrence of cerebral microhemorrhage depends on the antibody being used. Although 3D6, an N-terminal antibody with fibril plaque binding capacity, resulted in an increased incidence of microhemorrhage, 266, a mid-domain antibody without plaque binding, did not show such a liability signal in aged PDAPP transgenic mice after a 6-week dosing regimen (Racke et al., 2005). The authors suggest that the results indicate plaque binding is necessary for increased microhemorrhage to occur, although it is possible that 6 weeks of exposure was not enough to detect a treatment effect. Our results from the second 18-week longitudinal study further emphasize the complexity of these microhemorrhage mechanisms, because none were observed at the 6- and 12-week imaging time points during 8F5 treatment. The same antibody titer is expected across all treatment durations (although not measured in the current studies), although microhemorrhage was detected only at the 18-week time point. By taking the advantage of imaging in a longitudinal man-

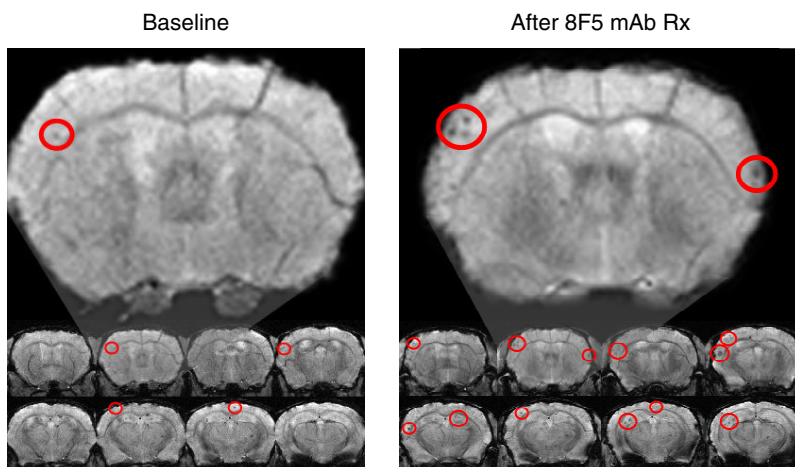


Fig. 9. One mouse that was excluded at the beginning of the 12-week longitudinal study (because of multiple abnormal MRI findings at baseline) revealed massive exacerbation of microhemorrhages (red circles) after 8F5 treatment. Second slices in the middle rows were magnified ($\sim 10\times$) for better visualization of microhemorrhage-induced hypointensity signal in MRI.

ner, we provide evidence that a sufficient antibody dosing duration, here 12 to 18 weeks, may be necessary for immunotherapy-induced cerebral microhemorrhage in aged Tg2576 mice. Nevertheless, the mechanisms involved in A β immunization-associated risk of cerebral hemorrhage warrant further investigation.

Despite the unknown mechanism by which immunotherapy may cause cerebral microhemorrhage, it seems that age is a significant factor. This is supported by the work of several groups showing microhemorrhage liability in different lines of APP transgenic mice over 19 months of age (Pfeifer et al., 2002; Wilcock et al., 2004, 2007; Racke et al., 2005), and others who reported no microhemorrhage signal in mice under 16 months of age (Pfeifer et al., 2002; Seabrook et al., 2006). In our second longitudinal study of 18 weeks in duration, we did not observe increased incidence of microhemorrhage until Tg2576 mice reached 21 months of age, illustrated in Fig. 6. By using a multiple time-point readout, our longitudinal MRI study provides the first direct evidence that age is an important factor for the development of cerebral microhemorrhage during immunotherapy. Significant development of CAA in aged transgenic mice (Pfeifer et al., 2002; Wilcock et al., 2004; Kumar-Singh et al., 2005; Racke et al., 2005) is presumably the cause, although spontaneous cerebral microhemorrhage in aged transgenic mice does occur (Kumar-Singh et al., 2005). This corroborates our baseline MRI findings of very few microhemorrhages (Figs. 4 and 7).

Because it is feasible to diagnose cerebral microhemorrhage in transgenic mice and humans using the T2*-weighted MRI technique, the success of A β immunotherapy may be improved by screening patients with Alzheimer's for the presence and severity of CAA and baseline microhemorrhages before such therapies are undertaken, especially for those patients undergoing treatment with anticoagulants. Although clinical trial findings with bapineuzumab in general showed good safety and tolerability, it is very important to note that all trials are excluding patients with cerebrovascular disease or MRI vascular abnormalities. Our findings in Tg2576 mice (Fig. 9) imply that patients with AD and preexisting cerebrovascular disease or MRI vascular abnormalities could be susceptible to severe adverse effects during immunotherapy.

In conclusion, a new preclinical safety biomarker for antibody-induced cerebral microhemorrhages is described. Anti-A β antibodies 6G1 and 8F5 increased the incidence of microhemorrhage in aged Tg2576 mice compared with baseline and vehicle-treated controls. This is the first example of exacerbation of cerebral microhemorrhages by a soluble oligomeric A β -selective antibody. A highly selective antibody for soluble oligomers that demonstrates little or no vascular plaque binding warrants further investigation. T2*-weighted MR microscopy can be readily applied to screening all A β -targeted immunotherapeutics in a longitudinal manner. This methodology can also be used in the evaluation of compounds directly targeting CAA, which is a disorder of growing societal importance and with few therapeutic options (Towfighi et al., 2005). Therefore, the information generated using this technology has the potential to directly translate to human clinical trials and thus may accelerate drug innovation.

References

Barghorn S, Nimmrich V, Striebinger A, Krantz C, Keller P, Janson B, Bahr M, Schmidt M, Bitner RS, Harlan J, et al. (2005) Globular amyloid β -peptide oligomer

- a homogenous and stable neuropathological protein in Alzheimer's disease. *J Neurochem* **95**:834–847.
- Boche D, Zotova E, Weller RO, Love S, Neal JW, Pickering RM, Wilkinson D, Holmes C, and Nicoll JA (2008) Consequence of A β immunization on the vasculature of human Alzheimer's disease brain. *Brain* **131**:3299–3310.
- Bradley WG Jr (1993) MR appearance of hemorrhage in the brain. *Radiology* **189**:15–26.
- Fazekas F, Kleinert R, Roob G, Kleinert G, Kapeller P, Schmidt R, and Hartung HP (1999) Histopathologic analysis of foci of signal loss on gradient-echo T2*-weighted MR images in patients with spontaneous intracerebral hemorrhage: evidence of microangiopathy-related microbleeds. *AJNR Am J Neuroradiol* **20**:637–642.
- Greenberg SM, Eng JA, Ning M, Smith EE, and Rosand J (2004) Hemorrhage burden predicts recurrent intracerebral hemorrhage after lobar hemorrhage. *Stroke* **35**:1415–1420.
- Hardy J and Selkoe DJ (2002) The amyloid hypothesis of Alzheimer's disease: progress and problems on the road to therapeutics. *Science* **297**:353–356.
- Hsiao K, Chapman P, Nilsen S, Eckman C, Harigaya Y, Younkin S, Yang F, and Cole G (1996) Correlative memory deficits, A β elevation, and amyloid plaques in transgenic mice. *Science* **274**:99–102.
- Jack CR Jr, Garwood M, Wengenack TM, Borowski B, Curran GL, Lin J, Adriani G, Gröhn OH, Grimm R, and Podusko JF (2004) In vivo visualization of Alzheimer's amyloid plaques by magnetic resonance imaging in transgenic mice without a contrast agent. *Magn Reson Med* **52**:1263–1271.
- Janus C, Pearson J, McLaurin J, Mathews PM, Jiang Y, Schmidt SD, Chishti MA, Horne P, Heslin D, French J, et al. (2000) A β peptide immunization reduces behavioural impairment and plaques in a model of Alzheimer's disease. *Nature* **408**:979–982.
- Kawarabayashi T, Younkin LH, Saido TC, Shoji M, Ashe KH, and Younkin SG (2001) Age-dependent changes in brain, CSF, and plasma amyloid (β) protein in the Tg2576 transgenic mouse model of Alzheimer's disease. *J Neurosci* **21**:372–381.
- Kumar-Singh S, Pirici D, McGowan E, Serneels S, Ceuterick C, Hardy J, Duff K, Dickson D, and Van Broeckhoven C (2005) Dense-core plaques in Tg2576 and PSAPP mouse models of Alzheimer's disease are centered on vessel walls. *Am J Pathol* **167**:527–543.
- Lee SP, Falangola MF, Nixon RA, Duff K, and Helpert JA (2004) Visualization of β -amyloid plaques in a transgenic mouse model of Alzheimer's disease using MR microscopy without contrast reagents. *Magn Reson Med* **52**:538–544.
- Linfante I, Llinas RH, Caplan LR, and Warach S (1999) MRI features of intracerebral hemorrhage within 2 hours from symptom onset. *Stroke* **30**:2263–2267.
- Luo F, Seifert TR, Edalji R, Loebbert RW, Hradil VP, Harlan J, Schmidt M, Nimmrich V, Cox BF, and Fox GB (2008) Noninvasive characterization of β -amyloid(1–40) vasoactivity by functional magnetic resonance imaging in mice. *Neuroscience* **155**:263–269.
- Morgan D, Diamond DM, Gottschall PE, Ugen KE, Dickey C, Hardy J, Duff K, Jantzen P, DiCarlo G, Wilcock D, et al. (2000) A β peptide vaccination prevents memory loss in an animal model of Alzheimer's disease. *Nature* **408**:982–985.
- Offenbacher H, Fazekas F, Schmidt R, Koch M, Fazekas G, and Kapeller P (1996) MR of cerebral abnormalities concomitant with primary intracerebral hematomas. *AJNR Am J Neuroradiol* **17**:573–578.
- Pfeifer M, Boncrisiano S, Bondolfi L, Stalder A, Deller T, Staufenbiel M, Mathews PM, and Jucker M (2002) Cerebral hemorrhage after passive anti-A β immunotherapy. *Science* **298**:1379.
- Racke MM, Boone LI, Hepburn DL, Parsadaian M, Bryan MT, Ness DK, Pirooz KS, Jordan WH, Brown DD, Hoffman WP, et al. (2005) Exacerbation of cerebral amyloid angiopathy-associated microhemorrhage in amyloid precursor protein transgenic mice by immunotherapy is dependent on antibody recognition of deposited forms of amyloid β . *J Neurosci* **25**:629–636.
- Salloway S, Sperling R, Gilman S, Fox NC, Blennow K, Raskind M, Sabbagh M, Honig LS, Doody R, van Dyck CH, et al. (2009) A phase 2 multiple ascending dose trial of bapineuzumab in mild to moderate Alzheimer disease. *Neurology* **73**:2061–2070.
- Schenk D (2002) Amyloid- β immunotherapy for Alzheimer's disease: the end of the beginning. *Nat Rev Neurosci* **3**:824–828.
- Schenk D, Barbour R, Dunn W, Gordon G, Grajeda H, Guido T, Hu K, Huang J, Johnson-Wood K, Khan K, et al. (1999) Immunization with amyloid- β attenuates Alzheimer-disease-like pathology in the PDAPP mouse. *Nature* **400**:173–177.
- Schroeter S, Khan K, Barbour R, Doan M, Chen M, Guido T, Gill D, Basi G, Schenk D, Seubert P, et al. (2008) Immunotherapy reduces vascular amyloid- β in PDAPP mice. *J Neurosci* **28**:6787–6793.
- Seabrook TJ, Jiang L, Thomas K, and Lemere CA (2006) Boosting with intranasal dendrimeric A β 1–15 but not A β 1–15 peptide leads to an effective immune response following a single injection of A β 1–40/42 in APP-tg mice. *J Neuroinflammation* **3**:14.
- Sigurðsson EM, Wadghiri YZ, Mosconi L, Blind JA, Knudsen E, Asuni A, Scholtzova H, Tsui WH, Li Y, Sadowski M, et al. (2008) A nontoxic ligand for voxel-based MRI analysis of plaques in AD transgenic mice. *Neurobiol Aging* **29**:836–847.
- Spires TL and Hyman BT (2005) Transgenic models of Alzheimer's disease: learning from animals. *NeuroRx* **2**:423–437.
- Thakker DR, Weatherspoon MR, Harrison J, Keene TE, Lane DS, Kaemmerer WF, Stewart GR, and Shafer LL (2009) Intracerebroventricular amyloid- β antibodies reduce cerebral amyloid angiopathy and associated micro-hemorrhages in aged Tg2576 mice. *Proc Natl Acad Sci USA* **106**:4501–4506.
- Towfighi A, Greenberg SM, and Rosand J (2005) Treatment and prevention of primary intracerebral hemorrhage. *Semin Neurol* **25**:445–452.
- Viswanathan A and Chabriat H (2006) Cerebral microhemorrhage. *Stroke* **37**:550–555.
- Weber R, Ramos-Cabrera P, Wiedermann D, van Camp N, and Hoehn M (2006) A fully noninvasive and robust experimental protocol for longitudinal fMRI studies in the rat. *NeuroImage* **29**:1303–1310.
- Wilcock DM, Jantzen PT, Li Q, Morgan D, and Gordon MN (2007) Amyloid- β

vaccination, but not nitro-nonsteroidal anti-inflammatory drug treatment, increases vascular amyloid and microhemorrhage while both reduce parenchymal amyloid. *Neuroscience* **144**:950–960.

Wilcock DM, Rojiani A, Rosenthal A, Subbarao S, Freeman MJ, Gordon MN, and Morgan D (2004) Passive immunotherapy against A β in aged APP-transgenic mice reverses cognitive deficits and depletes parenchymal amyloid deposits in spite of increased vascular amyloid and microhemorrhage. *J Neuroinflammation* **1**:24.

Zhang J, Yarowsky P, Gordon MN, Di Carlo G, Munireddy S, van Zijl PC, and Mori

S (2004) Detection of amyloid plaques in mouse models of Alzheimer's disease by magnetic resonance imaging. *Magn Reson Med* **51**:452–457.

Address correspondence to: Dr. Feng Luo, Translational Imaging and Biochemical Biomarkers, Global Pharmaceutical Research and Development, Abbott Laboratories, Dept. R4DF, Bldg AP4-2, 100 Abbott Park Road, Abbott Park, IL 60064. E-mail: feng.luo@abbott.com
